Spectrally Deconfounded Random Forests

Markus Ulmer, Cyrill Scheidegger*, and Peter Bühlmann
Serminar for Statistics, ETH Zürich

February 7, 2025

Abstract

We introduce a modification of Random Forests to estimate functions when unobserved confounding variables are present. The technique is tailored for high-dimensional settings with many observed covariates. We use spectral deconfounding techniques to minimize a deconfounded version of the least squares objective, resulting in the Spectrally Deconfounded Random Forests (*SDForests*). We show how the omitted variable bias gets small given some assumptions. We compare the performance of *SDForests* to classical Random Forests in a simulation study and a semi-synthetic setting using single-cell gene expression data. Empirical results suggest that *SDForests* outperform classical Random Forests in estimating the direct regression function, even if the theoretical assumptions, requiring linear and dense confounding, are not perfectly met, and that *SDForests* have comparable performance in the non-confounded case.

Keywords: Causal Inference, Confounding, High-dimensional setting, Omitted variable bias, Regression

---

1 Introduction

Random Forests (Breiman, 2001) and their variations, such as Random Survival Forests (Hothorn, 2005; Taylor, 2011), Quantile Regression Forests (Meinshausen, 2006), or distributional versions of Random Forests (Hothorn & Zeileis, 2021) are successfully applied to a wide range of datasets. In many cases of observational data, however, problems with "omitted variable bias" (Cinelli & Hazlett, 2020; Wilms et al., 2021) occur. This means that a bias is induced in estimating the relationships using standard Random Forests versions by not observing and including covariates that correlate with the other covariates and the response. In the setting of causality, this can be viewed as a confounded causal relationship with unobserved confounders (Pearl, 1980; Peters et al., 2016). A popular approach to deal with unobserved confounding is to use instrumental variables (IV) regression techniques (Bowden et al., 1990; Angrist et al., 1996; Stock & Trebbi, 2003). Finding enough strong and valid instrumental variables can be challenging, especially if many covariates with potential effects on the response are observed since the number of instruments must be as large as the number of effective covariates. Another possible way of reducing the hidden confounding bias, which we will adopt here, is to make some kind of "dense confounding effect" assumption, meaning that the non-observed factors or confounders affect most of the covariates. Then, a standard approach is to estimate the hidden confounding using methods from high-dimensional factor analysis (Bai, 2003) and explicitly adjust for them, see for example Leek and Storey (2007); Gagnon-Bartsch and Speed (2012); Fan et al. (2024) for approaches in this direction. Instead of estimating the latent factors explicitly, one can adjust for them implicitly using spectral transformations (Ćevid et al., 2020). Applying such spectral transformations, especially the trim transform, which we introduce later, does not require any tuning and is computationally very fast since it is a simple and explicit function of the singular value decomposition of the design matrix.

1.1 Our Contribution

Our contribution is a Random Forest algorithm that is able to address, at least partially, the problem of hidden confounding. Our proposal combines the great advantage and flexibility of standard Random Forests with spectral deconfounding techniques for dealing with the bias from unobserved factors or confounding. The latter was originally proposed for linear models by Ćevid et al. (2020); Guo et al. (2022) and was further developed for nonlinear additive models by Scheidegger et al. (2025). The application of spectral deconfounding techniques for Random Forests is novel.

We develop a new algorithm with R-package *SDModels* (Ulmer & Scheidegger, 2024) and show its performance in estimating the direct and unconfounded relationship between the observed covariates and the response. We demonstrate that in presence of hidden confounding, our method, the Spectrally Deconfounded Random Forest (*SDForest*), outperforms the standard Random Forests in many aspects. If no latent factor or confounding exists, our *SDForests* and standard Random Forests perform similarly, perhaps with a minimal edge in favor of the classical algorithm. Thus, if one is unsure whether hidden confounding is present, there is much to gain but not much to lose.

1.2 Notation

We denote the largest, the smallest, and i-th (non-zero) singular value of any rectangular matrix A by $\lambda_{\max}(A)$, $\lambda_{\min}(A)$ and $\lambda_i(A)$ respectively. The condition number is defined as $\text{cond}(A) := \frac{\lambda_{\max}(A)}{\lambda_{\min}(A)}$. Let $\{r_n\}_{n=1}^{\infty}$ and $\{k_n\}_{n=1}^{\infty}$ be positive constants. We use the notation $k_n := \Omega(r_n)$ if $\frac{r_n}{k_n} = \mathcal{O}(1)$, i.e., if k_n has asymptotically at least the same rate as r_n and $k_n \asymp r_n$ if k_n and r_n have asymptotically the same rate. We write $r_n \ll k_n$ if $\frac{r_n}{k_n} = o(1)$.

2 Confounding Model

Throughout this work, we assume the confounding model, written in terms of structural equations

$$
\begin{aligned}
X &\leftarrow \Gamma^T H + E \\
Y &\leftarrow f^0(X) + \delta^T H + \nu.
\end{aligned}
\tag{1}
$$

Here, $X \in \mathbb{R}^p$ are the predictors, $Y \in \mathbb{R}$ is the response and $H \in \mathbb{R}^q$ are unobserved hidden confounding factors. We assume that the confounder influences X with a linear effect $\Gamma \in \mathbb{R}^{q \times p}$ and Y with a linear effect $\delta \in \mathbb{R}^q$. Furthermore, ν is a random variable with mean zero and variance σ_ν^2, and E is a random vector with mean zero and covariance Σ_E, and E and H are uncorrelated. The error term E can be viewed as the unconfounded predictor if Γ equals zero. Finally, $f^0 \in \mathcal{F}$, where $\mathcal{F}$ is some class of functions from $\mathbb{R}^p$ to $\mathbb{R}$. The function f^0 encodes the direct causal relationship of interest, describing the causal relation of X on Y. The described model is visualized as a graph in Figure 1.
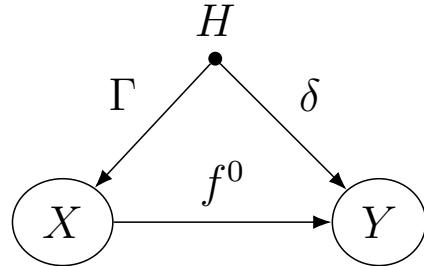

Figure 1: Confounding model (1), with hidden confounder H affecting X and Y linearly. The function $f^0(X)$ encodes the direct effect of X on Y.

3 Generic Methodology

We assume that we observe n i.i.d observations from X and Y generated by model (1). We concatenate them row-wise into the design matrix $\mathbf{X} \in \mathbb{R}^{n \times p}$ and the vector of responses $\mathbf{Y} \in \mathbb{R}^n$. Classical regression methods ignoring the confounding would estimate f^0 by minimizing the least squares objective $\hat{f} := \arg\min_{f \in \mathcal{F}} \|\mathbf{Y} - f(\mathbf{X})\|_2^2$, or a regularized version thereof, for a suitable class $\mathcal{F}$ of functions. This yields an estimate of $\arg\min_{f \in \mathcal{F}} \mathbb{E}[(Y - f(X))^2] = \mathbb{E}[Y|X] = f^0(X) + \delta^T \mathbb{E}[H|X]$, which is a biased estimate for f^0 in model (1). We apply a spectral transformation to the least squares objective to remove this confounding

bias. Let $Q \in \mathbb{R}^{n \times n}$ be a transformations matrix that depends on the data $\mathbf{X}$. Examples are the trim-transform and the PCA adjustment (Ćevid et al., 2020; Guo et al., 2022; Scheidegger et al., 2025). We use the trim-transform in our empirical results in Section 5, which limits all the singular values of $\mathbf{X}$ to some constant τ, but the methodology can be applied using other spectral transformations. Let $\mathbf{X} = UDV^T$ be the singular value decomposition of $\mathbf{X}$, where $U \in \mathbb{R}^{n \times r}$, $D \in \mathbb{R}^{r \times r}$, $V \in \mathbb{R}^{p \times r}$, where $r := \min(n, p)$ is the rank of $\mathbf{X}$. The trim transform Q is then defined as

$$Q := U\tilde{D}U^T \tag{2}$$

$$\tilde{D} := \begin{bmatrix} \tilde{d}_1/d_1 & 0 & \cdots & 0 \\ 0 & \tilde{d}_2/d_2 & \cdots & 0 \\ \vdots & \vdots & \ddots & \vdots \\ 0 & 0 & \cdots & \tilde{d}_r/d_r \end{bmatrix}$$

$$\tilde{d}_i := \min(d_i, \tau)$$

with τ being the median singular value of $\mathbf{X}$, as recommended by Ćevid et al. (2020). Trimming the first few singular values results in the reduction of the loss in the direction of the first few principal components of $\mathbf{X}$ and in the confounding model (1), this is also the direction containing most of the confounding effects. Reducing this part of the loss results in the reduction of the confounding bias. We will therefore minimize a spectrally transformed version of the mean squared error that we refer to as the spectral objective:

$$\min_{f \in \mathcal{F}} \frac{\|Q(\mathbf{Y} - f(\mathbf{X}))\|_2^2}{n}. \tag{3}$$

Theorem 1 below shows that if the confounding follows some assumptions and we have a spectral transformation, we optimize in the limit essentially $\min_{f \in \mathcal{F}} \|Q(f^0(\mathbf{X}) - f(\mathbf{X}) + \nu)\|_2^2/n$ with ν as in model (1) and being independent of X. This means that we asymptotically minimize a transformed least squares objective without confounding rather than the usual least squares objective with confounding. Figure 2 shows how the spectral transformation changes the correlation between $\mathbf{Y}$ and $f^0(\mathbf{X})$.

3.1 Assumptions and Technical Motivation

The spectral deconfounding methodology (Ćevid et al., 2020) relies on a set of assumptions that are also crucial for our *SDForests*. We review these assumptions in the following.

Model: The data is generated according to the confounding model (1) with

$$\mathbb{E}[H] = 0 \in \mathbb{R}^q, \ \mathbb{E}[E] = 0 \in \mathbb{R}^p, \ \mathbb{E}[HH^T] = I_q, \ \mathbb{E}[HE^T] = 0 \in \mathbb{R}^{p \times q}, \tag{4}$$

i.e., H and E are both centered, and they are uncorrelated. The assumption that H has unit covariance matrix is without loss of generality: let $\Sigma_H := \mathbb{E}[HH^T]$. We can then consider the confounding model with $\tilde{H} := \Sigma_H^{-1/2} H$, $\tilde{\Gamma} := \Sigma_H^{1/2} \Gamma$ and $\tilde{\delta} := \Sigma_H^{1/2} \delta$ which satisfies $\mathbb{E}[\tilde{H}\tilde{H}^T] = I_q$.
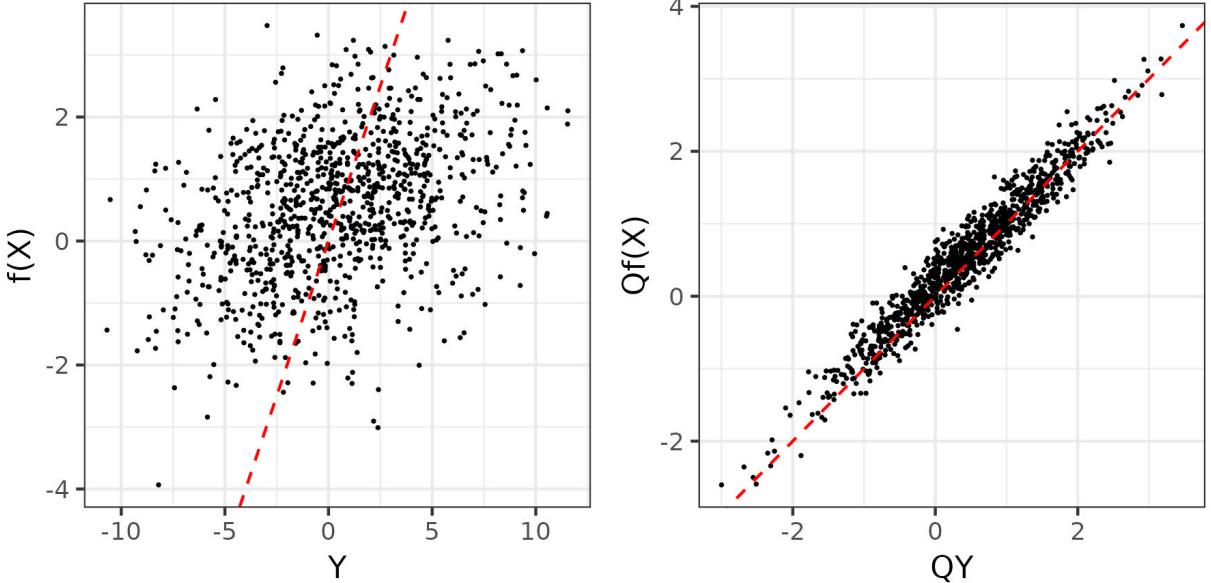
Figure 2: A random realization according to the confounding model (1) with non-linear f^0 as in (13) and with the same parameter as in Section 5. On the left we show $f^0(\mathbf{X})$ against $\mathbf{Y}$; on the right, the spectrally transformed versions are shown against each other, that is $Qf^0(\mathbf{X})$ versus $Q\mathbf{Y}$. In both visualizations, the line with a slope equal to one, which corresponds to perfect correlation, is shown in red.

Dimensions: We will see in Theorem 1 below that the confounding effect goes to zero as $\min(n,p)$ grows. Hence, we need to assume that p increases to infinity with n. Moreover, we need the number q of confounders to be low-dimensional, i.e., $q \ll \min(n,p)$.

Covariance of E: It is essential that the covariance $\Sigma_E := \mathbb{E}[EE^T] \in \mathbb{R}^{p \times p}$ of the un-confounded part E of X is sufficiently well-behaved. If, for example, E itself had a factor structure, it would be difficult to separate the confounding $\Gamma^T H$ from the factor structure in E. This well-behavedness assumption is formalized by

$$\mathrm{cond}(\Sigma_E) = \mathcal{O}(1) \text{ and } \lambda_{\max}(\Sigma_E) = \mathcal{O}(1). \tag{5}$$

A simple example where (5) is satisfied is when the components of E are uncorrelated and of the same order, i.e., $\Sigma_E = \mathrm{diag}(\sigma_1^2, \ldots, \sigma_p^2)$ with $\max_{i,j=1,\ldots,p} \sigma_i^2/\sigma_j^2 \leq C_1 < \infty$ and $\max_{i=1,\ldots,p} \sigma_i^2 \leq C_2 < \infty$ for some constants $C_1, C_2 > 0$ independent of p. However, more general covariance structures are possible.

Dense confounding: The dense confounding assumption intuitively means that each component of H affects many components of X and hence is a property of the matrix Γ. More formally, it is a statement on how large the minimal singular value of Γ should be. For Theorem 1 below, we will work under the assumption that

$$\lambda_{\min}(\Gamma) = \Omega(\sqrt{p}), \tag{6}$$

although weaker assumptions are possible (Guo et al., 2022; Scheidegger et al., 2025). Equation (6) is, for example, satisfied with high probability if $q/p \to 0$ and either

5

the rows or columns of Γ are sampled as i.i.d. sub-Gaussian random vectors with mean zero and covariance Σ_Γ with $\lambda_{\min}(\Sigma_\Gamma)$ bounded away from zero (see Lemma 6 in Ćevid et al. (2020)).

Spectral transformation: The spectral transformation Q defined in (2) (trim transform) satisfies

$$\lambda_{\max}(Q\mathbf{X}) = \mathcal{O}_P\left(\sqrt{\max(n,p)}\right). \tag{7}$$

In (Guo et al., 2022), (7) is verified for the case where E is a sub-Gaussian random vector and $\lambda_{\max}(\Sigma_E) = \mathcal{O}(1)$.

The following theorem, which is essentially a compilation of results from Ćevid et al. (2020) and Guo et al. (2022), serves as a motivation to construct *SDForests* based on the spectral objective (3).

Theorem 1. *Assume the confounding model (1) and assume that the conditions (4), (5), (6) and (7) hold. Then, it holds that*

$$\frac{\|Q(\mathbf{Y} - f(\mathbf{X}))\|_2}{\sqrt{n}} = \frac{\|Q(f^0(\mathbf{X}) - f(\mathbf{X}) + \nu)\|_2}{\sqrt{n}} + R_n$$

where $R_n = \mathcal{O}_{\mathbb{P}}\left(\frac{\|\delta\|_2}{\min(\sqrt{n},\sqrt{p})}\right)$.

In particular, if $\|\delta\|_2^2 \ll \min(n,p)$, we have that $R_n = o_P(1)$. The condition $\|\delta\|_2^2 \ll \min(n,p)$ holds for example if $q \ll \min(n,p)$ and all the entries of $\delta \in \mathbb{R}^q$ are bounded.

4 *SDForest* Algorithm

In principle, our algorithm works similarly to the original CART algorithm (Li et al., 1984) and Random Forests (Breiman, 2001). The main difference is that we minimize the spectral objective (3) instead of the classical mean squared error. This results in additional challenges. For example, we can no longer decompose the loss and treat leaves independently but must estimate tree levels globally using linear regression, as explained next.

4.1 Spectrally Deconfounded Tree

Assume the confounding model (1) with $\mathcal{F}$ being the function class of step functions, e.g.,

$$f^0(X) := \sum_{m=1}^{M} \mathbb{1}_{\{X \in R_m\}} c_m, \tag{8}$$

where $(R_m)_{m=1}^M$ are regions dividing the space of $\mathbb{R}^p$ into M rectangular parts. Each region has response level $c_m \in \mathbb{R}$. We can write the sample version as $f^0(\mathbf{X}) = \mathcal{P}c$ where $\mathcal{P} \in \{0,1\}^{n \times M}$ is an indicator matrix encoding to which region an observation belongs, i.e. $\mathcal{P}_{i,m} = 1$ if the ith row of $\mathbf{X}$ belongs to R_m and $\mathcal{P}_{i,m} = 0$ otherwise. The vector $c = (c_1, \ldots, c_M) \in \mathbb{R}^M$ contains the levels corresponding to the different regions. We can estimate $\hat{f}$ in the spirit of (3) with

$$(\hat{\mathcal{P}}, \hat{c}) := \arg \min_{\mathcal{P}' \in \{0,1\}^{n \times M}, c' \in \mathbb{R}^M} \frac{\|Q(\mathbf{Y} - \mathcal{P}'c')\|_2^2}{n}, \tag{9}$$

where $\mathcal{P}'$ has to follow a repeated splitting of the space of $\mathbb{R}^p$ into rectangular regions. M is fixed here but has to be estimated in practice. $\hat{M}$ also has to be regularized so that it does not go to n, and we overfit by having a region for each observation. If the partition $\mathcal{P}$ is known, the spectral objective (3) becomes

$$\begin{aligned}\hat{c} &= \arg \min_{c' \in \mathbb{R}^M} \frac{\|Q(\mathbf{Y} - \mathcal{P}c')\|_2^2}{n} \\ &= \arg \min_{c' \in \mathbb{R}^M} \frac{\|\tilde{\mathbf{Y}} - \tilde{\mathcal{P}}c'\|_2^2}{n},\end{aligned} \tag{10}$$

where $\tilde{\mathbf{Y}} := Q\mathbf{Y}$ and $\tilde{\mathcal{P}} := Q\mathcal{P}$. This is a linear regression problem, and we estimate c by

$$\hat{c} = (\tilde{\mathcal{P}}^T \tilde{\mathcal{P}})^{-1} \tilde{\mathcal{P}}^T \tilde{\mathbf{Y}}. \tag{11}$$

This contrasts the classical CART setting, where, given a partition $\mathcal{P}$, we estimate c with the mean per region μ_m. In Equation (10), each $\hat{c}_m$ depends not only on the observations belonging to R_m but on all the observations due to the rotation and scaling of the spectral transformation. For estimating $\hat{\mathcal{P}}$ we propose Algorithm 1. Algorithm 1 estimates the partition using a tree structure and a repeated splitting of leaves. Since comparing all possibilities for $\mathcal{P}$ is impossible, we let a tree grow greedily. Given the current tree, we iterate over all regions and all possible splits. We choose the one that reduces the spectral loss (9) the most, using a subroutine described in Section 4.2, and estimate after each split all the region estimates $\hat{c}$ using Equation (10) on line 15. In lines 4-10, we estimate the potential loss decrease only for the two new regions $\mathcal{B} = (b^*, M + 1)$. We reuse previously estimated loss decreases for potential splits in the other regions. Because the spectral transformation Q induces dependency between the observations, the regions are not independent in contrast to the classical setting. The loss-decrease for a potential split changes after another split in another region. Despite this, we reuse the previously estimated loss decrease to save computation time and argue that the change is small and still results in a reasonable split; see also Figure 9. This is repeated until the loss decreases less than a minimum loss decrease after a split. The minimum loss decrease equals a cost-complexity parameter cp times the initial loss when only an overall mean is estimated. The cost-complexity parameter cp controls the complexity of a regression tree and acts as a regularization parameter. This should stop $\widehat{M}$ from growing up to n. Algorithm 1 results in a regression tree that has been grown to minimize the spectral loss (9) and unbiased response levels following Equation (10).

4.2 Subroutine

In the Mth iteration of Algorithm 1, we have the indicator matrix $\hat{\mathcal{P}} = \hat{\mathcal{P}}^M \in \{0,1\}^{n \times M}$ with entries $\hat{\mathcal{P}}_{i,m}^M = 1$ if and only if the ith observation lies in region m. We encode a candidate split in the region b of the partition using covariate j at the splitting value s by $e \in \{0,1\}^n$ where e must be in the support of the bth column of $\hat{\mathcal{P}}^M$ (i.e. the indices of 1s in

e are a subset of the indices of 1s of the bth column of $\hat{\mathcal{P}}^M$)) and the entries depend on j and s. A candidate split results then in a candidate partition $\mathcal{P}^{M+1}(e)$ with $M-1$ columns equal to columns $\hat{\mathcal{P}}^M$, the bth column equal to the bth column of $\hat{P}^M$ minus e and an additional column equal to e. In lines 4-10 of Algorithm 1, we seek to find the optimal e among a large number of candidate splits such that the spectral objective $\|QY - Q\mathcal{P}^{M+1}(e)\hat{c}\|_2^2$ is minimal, where $\hat{c}$ is the least squares estimator $\hat{c} := \arg\min_{c \in \mathbb{R}^{M+1}} \|QY - Q\mathcal{P}^{M+1}(e)c\|_2^2$. Naively, for every candidate e, one would update the indicator matrix $\hat{\mathcal{P}}$, calculate the corresponding least squares estimator $\hat{c}$ and plug it in to obtain the loss decrease. Using the following procedure, the decrease in loss can be calculated more efficiently.

Note that $\text{span}(Q\mathcal{P}^{M+1}(e)) = \text{span}(Q\hat{\mathcal{P}}^M, Qe)$. We set $u_1' := Q \cdot (1, \ldots, 1)^T$ and $u_1 := u_1'/\|u_1'\|_2$. We proceed by induction and assume that we already have $u_2, \ldots, u_M$ such that $(u_1, \ldots, u_M)$ form an orthonormal basis for $\text{span}(Q\hat{\mathcal{P}}^M)$. Consequently, $\text{span}(Q\mathcal{P}^{M+1}(e)) = \text{span}(Q\hat{\mathcal{P}}^M, Qe) = \text{span}(u_1, \ldots, u_M, Qe) = \text{span}(u_1, \ldots, u_M, u_{M+1}(e))$, where we use orthogonalization to obtain $u_{M+1}(e)$, i.e. $u_{M+1}(e) = u_{M+1}(e)'/\|u_{M+1}(e)'\|_2$ with $u_{M+1}(e)' = Qe - \sum_{l=1}^M (u_l^T Qe)u_l = (Q - \sum_{l=1}^M u_l u_l^T Q)e$.

Let $\Pi_{M+1}(e) \in \mathbb{R}^{n \times n}$ be the orthogonal projection on $\text{span}(Q\mathcal{P}^{M+1}(e)) = \text{span}(Q\hat{\mathcal{P}}^M, Qe) = \text{span}(u_1, \ldots, u_M, u_{M+1}(e))$. We seek for e that minimizes $\|QY - Q\mathcal{P}^{M+1}(e)\hat{c}\|_2^2 = \|(I_n - \Pi_{M+1}(e))Q\mathbf{Y}\|_2^2$. But because $(u_1, \ldots, u_M, u_{M+1}(e))$ is an orthonormal set, it follows that

$$\|(I_n - \Pi_{M+1}(e))Q\mathbf{Y}\|_2^2 = \|Q\mathbf{Y}\|_2^2 - \|\Pi_{M+1}(e))Q\mathbf{Y}\|_2^2 = \|Q\mathbf{Y}\|_2^2 - \sum_{l=1}^M (u_l^T Q\mathbf{Y})^2 - (u_{M+1}(e)^T Q\mathbf{Y})^2.$$

To find the optimal split e, it suffices to maximize $\alpha(e) := (u_{M+1}(e)^T Q\mathbf{Y})^2$ among the candidate splits. Once the optimal split e^* is found, one can define $u_{M+1} := u_{M+1}(e^*)$ and $\hat{\mathcal{P}}^{M+1} := \mathcal{P}^{M+1}(e^*)$ and proceed with step $M + 2$.

4.3   Spectrally Deconfounded Random Forests

The next natural step is to use the spectrally deconfounded regression trees (SDTree) to build spectrally deconfounded Random Forests (*SDForests*) to estimate arbitrary functions. Random Forests have been introduced in (Breiman, 2001) and proven really powerful. The idea is to combine multiple regression trees into an ensemble in order to decrease variance and get a smoother function. Ensembles work best if the different models are independent of each other. To decorrelate the regression trees as much as possible from each other, we have two mechanisms. The first one is bagging (Breiman, 1996), where we train each regression tree on an independent bootstrap sample of the observations, i.e., we draw a random sample of size n with replacement from the observations. The second mechanic to decrease the correlation is that only a random subset of the covariates is available for each split. Before each split, we sample mtry $\leq p$ from all the covariates and choose the one that reduces the loss the most from those. Since we already have Algorithm 1, it only takes minor changes to build an *SDForest* with it. In Algorithm 1 before line 11, we sample a set p_{mtry} of size mtry from the covariates and in line 11, we only check in this set of randomly sampled covariates for the best split, e.g., $j \in p_{\text{mtry}}$. This procedure gives the spectrally deconfounded Random Forest in Algorithm 2. We predict with all the trees separately and use the mean over all trees as the Random Forest prediction. This gives the estimated function

---

Algorithm 1 Spectrally Deconfounded Regression Tree

1: **Inputs:**
   $\mathbf{X} \in \mathbb{R}^{n \times p}$, $\mathbf{Y} \in \mathbb{R}^n$, $Q \in \mathbb{R}^{n \times n}$, $\mathsf{cp} \in \mathbb{R}$, $M_{max} \in \mathbb{N}$

2: **Initialize:**
   $M \leftarrow 1$
   $\hat{\mathcal{P}} \leftarrow (1, \dots, 1)^T \in \mathbb{R}^{n \times 1}$
   $\tilde{\hat{\mathcal{P}}} \leftarrow Q\hat{\mathcal{P}}$
   $\tilde{\mathbf{Y}} \leftarrow Q\mathbf{Y}$
   $u \leftarrow \hat{\mathcal{P}}/\|\hat{\mathcal{P}}\|_2$
   $Q^d \leftarrow Q - uu^T Q$
   $\hat{c} \in \mathbb{R}^M \leftarrow \arg\min_{c' \in \mathbb{R}^m} \|\tilde{\mathbf{Y}} - \tilde{\hat{\mathcal{P}}} c'\|_2^2/n$
   $l^{init} \leftarrow l^{temp} \leftarrow \|\tilde{\mathbf{Y}} - \tilde{\hat{\mathcal{P}}} \hat{c}\|_2^2/n$
   $l^{dec} \in \mathbb{R}^M \leftarrow 0$
   $\mathcal{B} \leftarrow 1$

3: **for** $M = 1$ to M_{max} **do**
4:     **for** b in $\mathcal{B}$ **do**   ▷ subroutine
5:        **for** (j, s) in potential splits in region b **do**
6:           $e_{b,j,s} \in \{0, 1\}^n \leftarrow$ indices of samples belonging to the new partition
7:           $u \leftarrow Q^d e_{b,j,s}/\|Q^d e_{b,j,s}\|_2$
8:           $\alpha_{b,j,s} \leftarrow (u^T \tilde{\mathbf{Y}})^2$
9:        **end for**
10:    **end for**
11:    $(b^*, j^*, s^*) \leftarrow \arg\max \alpha_{b,j,s}$ ▷ optimal split over $b \in \{1, \dots, M\}$
12:    $u \leftarrow Q^d e_{b^*,j^*,s^*}/\|Q^d e_{b^*,j^*,s^*}\|_2$
13:    $Q^d \leftarrow Q^d - uu^T Q$
14:    $\hat{\mathcal{P}}^* \leftarrow$ splitting $\hat{\mathcal{P}}$ at (b^*, j^*, s^*) ▷ resulting in $\hat{\mathcal{P}}^* \in \mathbb{R}^{n \times (M+1)}$
15:    $\hat{c}^* \leftarrow \arg\min_{c' \in \mathbb{R}^M} \|\tilde{\mathbf{Y}} - \tilde{\hat{\mathcal{P}}}^* c'\|_2^2/n$
16:    $l^* \leftarrow \|\tilde{\mathbf{Y}} - \tilde{\hat{\mathcal{P}}}^* \hat{c}^*\|_2^2/n$
17:    $d \leftarrow l^{temp} - l^*$
18:    **if** $d > \mathsf{cp} * l^{init}$ **then**
19:       $\hat{\mathcal{P}} \leftarrow \hat{\mathcal{P}}^*$
20:       $\hat{c} \leftarrow \hat{c}$
21:       $l^{temp} \leftarrow l^*$
22:       $\mathcal{B} \leftarrow (b^*, M+1)$ ▷ the new partitions
23:    **else**
24:       break
25:    **end if**
26: **end for**

$$\hat{f}(X) := \frac{1}{N_{tree}} \sum_{t=1}^{N_{tree}} SDTree_t(X). \tag{12}$$

Algorithm 2 Spectrally deconfounded Random Forest

Inputs:
$\quad$ $\mathbf{X} \in \mathbb{R}^{n \times p}$, $\mathbf{Y} \in \mathbb{R}^n$, $Q \in \mathbb{R}^{n \times n}$, $N_{tree} \in \mathbb{N}$, mtry $\in [1, p]$
$\quad$ **for** $t = 1$ to N_{tree} **do**
$\quad\quad$ $X^t \leftarrow$ bootstrap sample of X
$\quad\quad$ $SDtree_t \leftarrow$ SDTree from Algorithm 1 with random set of covariates of size mtry at each split using X^t
$\quad$ **end for**

---

5   Empirical Results

For the simulation study, we simulate data according to the confounding model (1) with a random f^0 using the Fourier basis

$$f^0(X) := \sum_{j=1}^{p} \mathbb{1}_{\{j \in \mathcal{J}_s\}} \sum_{k=1}^{K} a_{j,k} \cos(0.2k \cdot x_j) + b_{j,k} \sin(0.2k \cdot x_j) \tag{13}$$

where $\mathcal{J}_s$ is a random subset of $1, \ldots, p$ of size four being the parents of Y (among the X variables). We simulate with $n = 1000$, $p = 500$, and $q = 20$. The entries of $\mathbf{E} \in \mathbb{R}^{n \times p}$, $\mathbf{H} \in \mathbb{R}^{n \times q}$, $\delta \in \mathbb{R}^q$, and $\Gamma \in \mathbb{R}^{q \times p}$ are sampled i.i.d. from a Gaussian with expectation zero and $\sigma = 1$. The additional noise $\nu \in \mathbb{R}^n$ is sampled i.i.d. from a Gaussian with mean zero and $\sigma_\nu = 0.1$. For the four causal parents, we sample the coefficients $a_{j,k}$ and $b_{j,k}$ uniformly on $[-1, 1]$ with fix the number of basis functions $K = 2$ for the additive function.

We use the *SDForest* with a hundred trees, mtry $= \lfloor 0.5p \rfloor$ and Q as the trim-transform (2) (Ćevid et al., 2020) to estimate the causal function. We compare the results of the *SDForest* to the estimated function by the classical Random Forest using the r package *ranger* (Wright & Ziegler, 2017).

In Figure 3, we compare the variable importance of the *SDForest* and the classical Random Forest for one simulation run. The variable importance of a covariate is calculated as the sum of the loss decrease resulting from all splits that divide a region using that covariate. The mean of the variable importance of all trees results in the variable importance for the forest. For the *SDForest*, we report the reduction of the spectral loss (3) instead of the MSE. For the *SDForest*, the four most important covariates are also the four true causal parents of Y. Three of those also have a clear separation from the remaining 497 covariates. For the classical Random Forest, the variable importance for the true causal parents lies within the bulk of spurious covariates. The most important covariate among the true causal parents is only on rank 134 and we would have to use almost all the covariates to include all the causal parents in the selected set.

Instead of examining the variable importance of the fully grown trees in the *SDForest*, we can also examine the regularization paths of the covariates. Figure 4 shows on the left
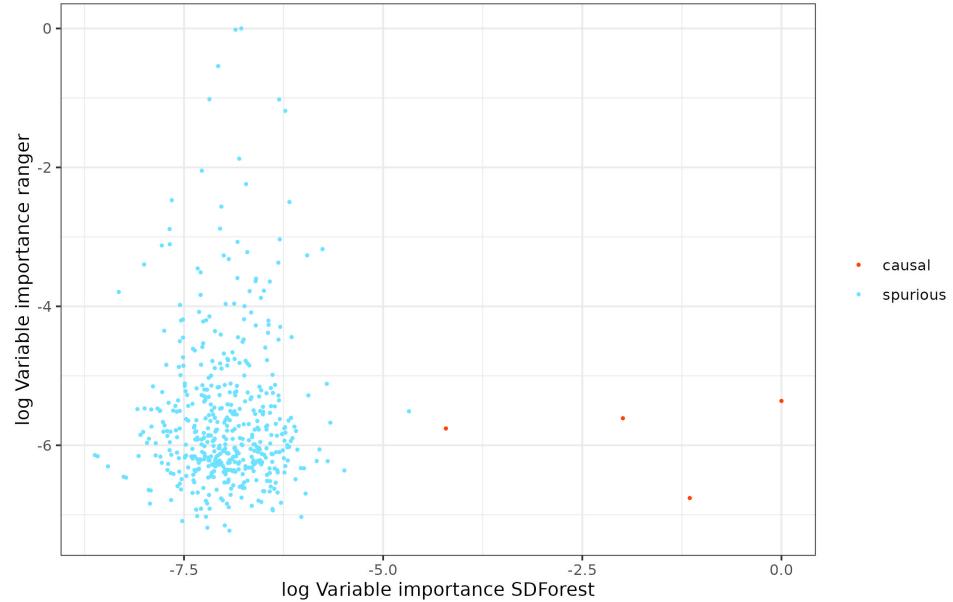
Figure 3: Comparison of variable importance for a realization of model (13) between the classical Random Forest estimated by *ranger* and the *SDForest*. The variable importance for both methods is scaled to the interval $[0, 1]$ and log-transformed. The true causal parents of the response Y are marked in red.

side the variable importance for the *SDForest* against increasing regularization, where one increases cp subsequently pruning the trees. Here again, three of the causal parents appear. On the right side in Figure 4, we show stability selection (Meinshausen & Bühlmann, 2010), where Π is the ratio of trees that use a particular covariate in the forest given increasing regularization. In the stability selection paths, we also see the fourth causal parent.

In addition to screening for the sparse causal set among a large number of covariates, we can also look at the functional dependence of the response Y on the causal parents. We use partial dependence plots (Friedman, 2001) to visualize the partial dependence. The idea is to predict $\hat{f}(\mathbf{X})$ for each observation and vary $\mathbf{X}_j$ on an interval while we keep the other covariates at the observed values. This gives for every observation a different function of X_j. The mean over all the observations can then be shown as a representative marginal effect of X_j on the response Y. Figure 5 shows how the *SDForest* estimates the true causal function. Especially for covariate 195, the estimated function approximates the true function well. Covariate 183, the covariate with only slightly higher importance than the bulk of spurious covariates, has almost a constant influence on Y. This shows some limitations of estimating a sparse causal relationship in the presence of hidden confounding and high dimensionality. Such a nuanced true function as for variable 183 might be hard to estimate with the additional disturbance of confounding and noise. The classical Random Forest distributes the estimated function among all the spurious covariates and estimates almost a constant function for all four causal parents. The partial dependence plots for the estimated classical Random Forest are shown in Figure 6.
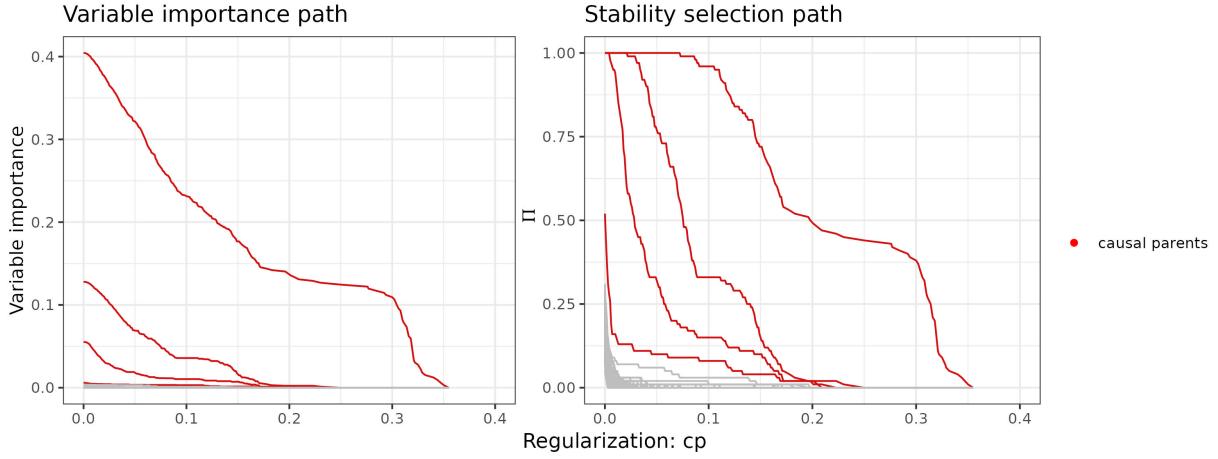
Figure 4: Regularization paths of the *SDForest* estimated on a realization of model (13) when varying the cost-complexity parameter `cp` resulting in more or less pruned trees. Each curve corresponds to a single covariate. On the left side are the variable importance paths for different strengths of regularization shown. On the right side are the stability selection paths against the strength of regularization shown. Π corresponds to the ratio of trees in the forest that use a covariate. The truly causal parents of the response Y correspond to the red curves.

5.1 Performance of *SDForests*

To quantify the performance of the *SDForests* in estimating the causal function, we perform simulation studies varying the different dimensions in the simulation. The default dimensions are $n = 500$, $p = 500$, and $q = 20$, and we randomly draw data according to model (13). Each of those dimensions is varied separately to estimate the dependence of the performance on these different factors. Every experiment is repeated 200 times, where every time, the whole data-generating process is newly drawn at random. The performance is measured by the mean distance of the true causal function and the estimated function evaluated at 500 test observations $f_{mse} := \frac{1}{n_{test}} \sum_{i=1}^{n_{test}} (f^0(x_{test,i}) - \hat{f}(x_{test,i}))^2$. The performance of the *SDForests* and the classical Random Forests depending on different dimensions is shown in Figure 7. Theorem 1 shows how the spectral objective (3) behaves as the dimensionality p, and the number of observations n grows to infinity. The term R_n goes asymptotically with $\min(\sqrt{n}, \sqrt{p})$ to zero. So, we need both n and p to grow for consistency. With this simulation study, we look at the dependence of the performance on those quantities in practice. Figure 7a shows the error distribution depending on the sample size. The *SDForests* perform clearly better in estimating the causal function, and the error decreases with a larger sample size. We see the dependence of the performance on the number of covariates in Figure 7b. At $p > 20$, we see how the *SDForests* start to perform significantly better than the classical Random Forests. When increasing p above 50, the error no longer seems to decrease, which hints that there is a certain threshold of p after which deconfounding is successful. Even with only the four causal parents as covariates, the *SDForests* do not perform worse than the classical versions, and we really do not seem to lose anything with *SDForests*, even in low-dimensional settings. With stronger confounding, estimating the causal function becomes increasingly difficult. Not only does
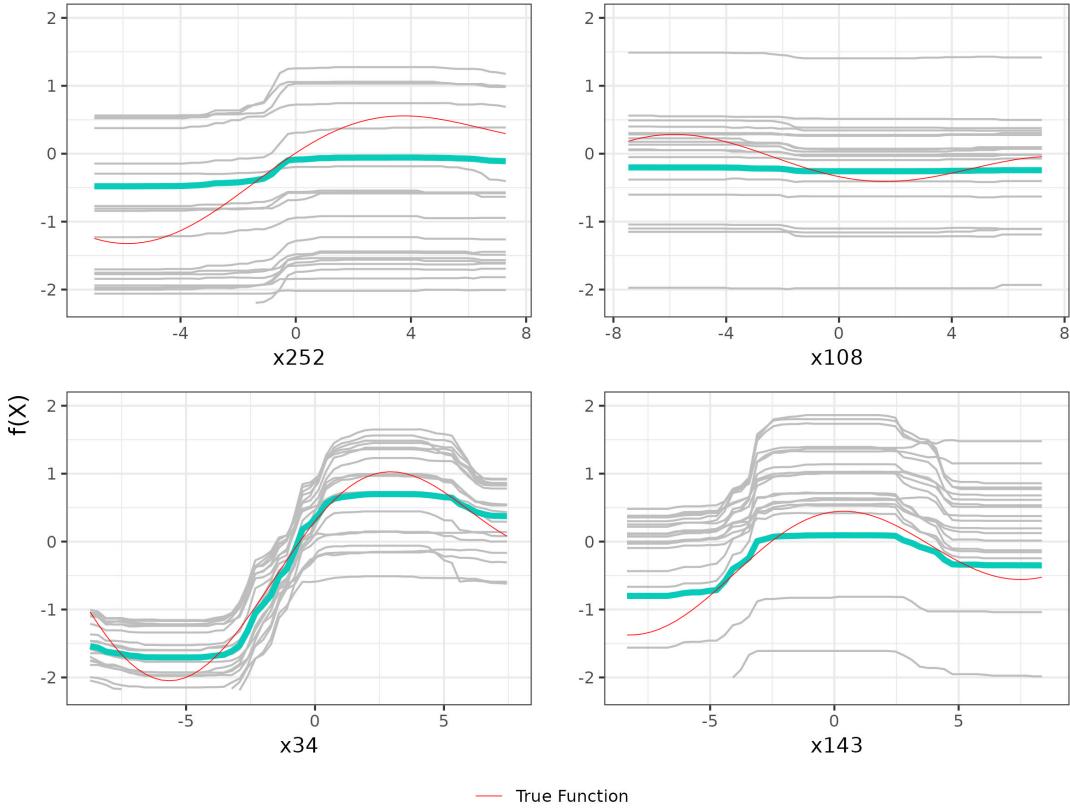
Figure 5: Partial dependence plots of the estimated *SDForest* for the four true causal parents of the response Y. In red is the corresponding true partial causal function. The grey lines show the observed empirical partial functions for 19 randomly selected observations, and the green line is the average of all observed partial functions.
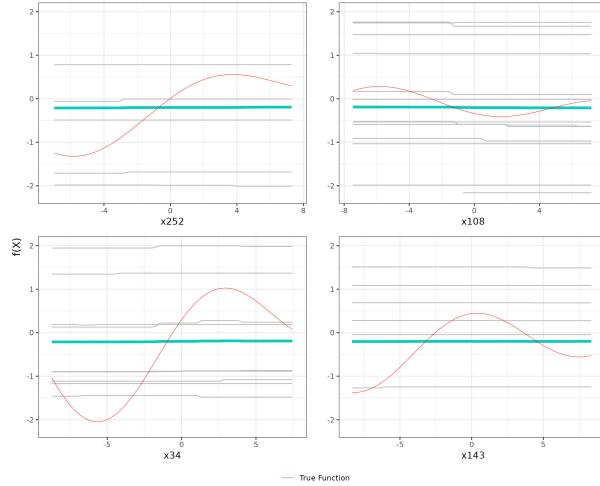

Figure 6: Partial dependence plots as in Figure 5 but now with the estimated classical Random Forest by *ranger* for the four true causal parents of the response Y. The classical Random Forest essentially leads to constant functions, whereas the true lines (in red) are varying.

the bias increase but so does the variance in the response. Therefore, we expect the error to increase with increasing confounding even for the *SDForests*. Figure 7c shows this behavior with a simulation study, where we increase the number of confounding variables. For $q = 0$, the setting corresponds to the classical model without confounding, and both the classical Random Forests and the *SDForests* perform really well. It is important to note that we do not lose much, even when the data is not confounded, by applying the spectral deconfounding. However, as can be seen for increasing confounding, we can gain a lot if there is hidden confounding present. In Figure 7d, we follow up on the assumption of dense confounding. Here, instead of having random effects of the confounders on all the covariates, we simulate the data with only a random subsample of the covariates being affected by confounding. The denser the confounding becomes, the better *SDForests* perform. With around 200 covariates affected (40%), the *SDForests* start performing similarly as if there were no confounding, while with sparser confounding, *SDForest* still outperforms *ranger*.

6   Single-Cell Data

We apply *SDForest* and *ranger* to Single-cell gene expression data to compare the resulting model on the scRNA-seq dataset for the cell RPE1 generated by Replogle et al. (2022). We use the preprocessed and filtered dataset provided by Chevalley et al. (2022). As the response, we choose the gene for EIF1 following the arguments of Shen et al. (2023) conjecturing that EIF1 might be a leaf node in the causal graph of genes. Using the observational data without any interventional gene knockouts ($n = 11485$ observations), we use all the other gene expressions ($p = 382$) as predictors and fit both *ranger* and *SDForest*. For both methods, we fit 500 trees using default parameters. To test for robustness against dense confounding, we synthetically perturb the original cleaned and filtered dataset. For this, we construct $\mathbf{X}_\tau := \mathbf{X} + \mathbf{H}\Gamma\tau$ and $\mathbf{Y}_\tau := Y + \mathbf{H}\delta\tau$, where $\mathbf{Y}$ is the original expression of EIF1 and $\mathbf{X}$ are the other original gene expressions used for prediction. The entries of $\mathbf{H} \in \mathbb{R}^n$, $\Gamma \in \mathbb{R}^{1\times 382}$, and $\delta \in \mathbb{R}$ are sampled i.i.d. from $\mathcal{N}(0, 1)$ while we vary τ to increase the added dense confounding. We fit both methods to $\mathbf{X}_\tau$ and $\mathbf{Y}_\tau$ with increasing τ and analyze how much the estimated functions change. The change in the estimated functions is calculated as the change of the out-of-bag predictions of $f_\tau^{ranger}(\mathbf{X}^\tau)$ and $f_\tau^{\mathrm{SDF}}(\mathbf{X}^\tau)$ depending on τ

$$\frac{\|f_\tau^{\mathrm{method}}(\mathbf{X}_\tau) - f_0^{\mathrm{method}}(\mathbf{X}_0)\|_2^2}{n}.$$

We repeat the synthetic confounding of the data by sampling 20 times $\mathbf{H}$, Γ, and δ and increasing τ. The distributions of the function changes are shown in Figure 8. With no added confounding, the difference between the two functions is small (see caption of Figure 8). When increasingly adding dense confounding, we clearly see how the estimated function by *ranger* changes, while *SDForest* shows robustness against this added perturbation.

7   Conclusion

We propose the Spectrally Deconfounded Random Forest algorithm *SDForest* with R-package *SDModels* (Ulmer & Scheidegger, 2024) to estimate direct regression functions in high-dimensional data in the presence of dense hidden confounding. This can be used to
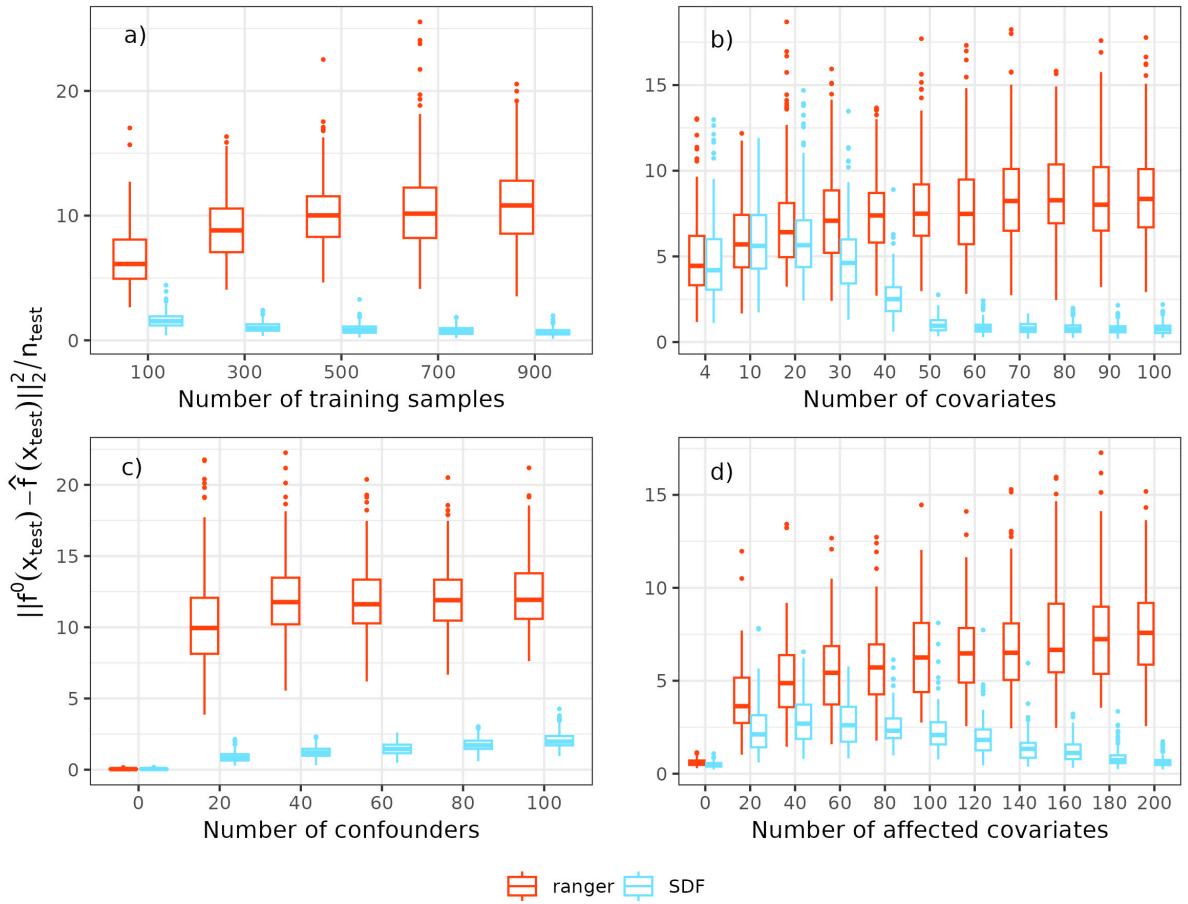
Figure 7: Mean squared error of the estimated causal function $\hat{f}(X)$ by classical Random Forests estimated by *ranger* and the *SDForests* depending on different simulation parameters. In subfigure a), we show how the performance depends on the sample size. In subfigure b), we show how the performance depends on the dimensionality of the observed data. The dependence of the performance on the amount of confounding is shown in subfigure c), where zero confounders corresponds to the classical setting without confounding. Subfigure d) shows the dependency of the performance on the number of affected covariates by the confounding, investigating the importance of dense confounding.

screen for relevant covariates among a large set of variables, and the procedure provides robustness against unobserved confounding, gaining much in the confounded case but losing little if no confounding is present. *SDModels* provides functions such as regularization paths and stability selection to screen for relevant covariates as well as partial dependence plots to understand their relation to the variable of interest. We demonstrate the empirical behavior of *SDForests* for different settings, including also difficult cases with sparse confounding to illustrate some fundamental limitations (but not found to be clearly worse than classical Random Forests).
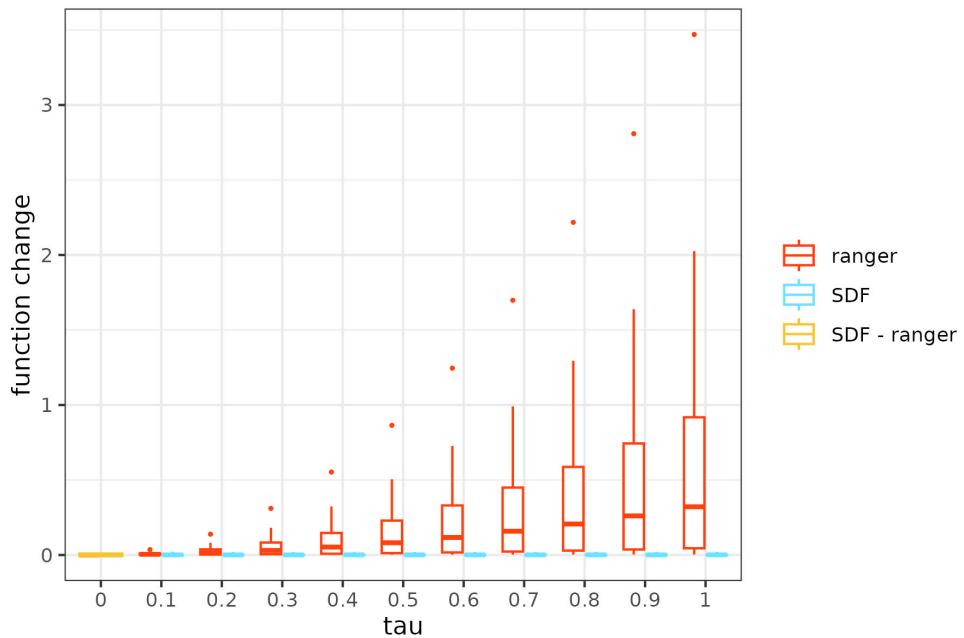
Figure 8: Change in prediction $\frac{\|f_\tau^{\text{method}}(\mathbf{X}_\tau) - f_0^{\text{method}}(\mathbf{X}_0)\|_2^2}{n}$ of *ranger* and *SDForest* when perturbing the data with additional dense confounding. At $\tau = 0$ and in yellow, we show the initial difference in prediction of *ranger* and *SDForest* when estimating and predicting on the unperturbed data $\frac{\|f_0^{\text{SDF}}(\mathbf{X}_0) - f_0^{ranger}(\mathbf{X}_0)\|_2^2}{n} = 0.0016$.
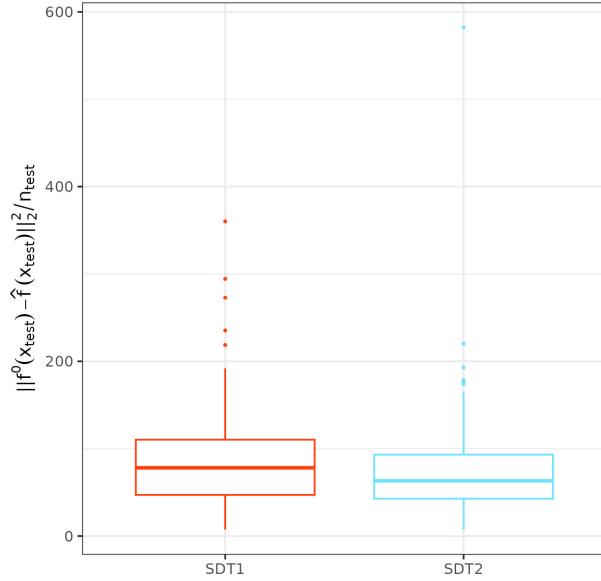
8 Additional Figures

Figure 9: Mean squared error of the estimated causal function $\hat{f}(X)$ by SDTree. SDT1 corresponds to Algorithm 1 while SDT2 uses $\mathcal{B} \leftarrow (1, \ldots, M+1)$ in line 22 instead of only the new partitions. The data is simulated using the confounding model (1) and with the same parameter as in Section 5 but using a random regression tree for f^0 as in (8).

9 Proofs

Theorem 1. *Assume the confounding model (1) and assume that the conditions* (4), (5), (6) *and* (7) *hold. Then, it holds that*

$$\frac{\|Q(\mathbf{Y} - f(\mathbf{X}))\|_2}{\sqrt{n}} = \frac{\|Q(f^0(\mathbf{X}) - f(\mathbf{X}) + \nu)\|_2}{\sqrt{n}} + R_n$$

where $R_n = \mathcal{O}_{\mathbb{P}} \left(\frac{\|\delta\|_2}{\min(\sqrt{n}, \sqrt{p})} \right).$

Proof. As in (Guo et al., 2022) and (Ćevid et al., 2020), let $b = \arg\min_{b' \in \mathbb{R}^p} \mathbb{E}[(X^T b' - H^T \delta)^2] = \mathbb{E}[XX^T]^{-1} \mathbb{E}[XH^T \delta]$, i.e. $X^T b$ is the L_2 projection of $H^T \delta$ onto X. By (1) and

the triangle inequality, we have that

$$
\left| \frac{\|Q(\mathbf{Y} - f(\mathbf{X}))\|_2}{\sqrt{n}} - \frac{\|Q(f^0(\mathbf{X}) - f(\mathbf{X}) + \nu)\|_2}{\sqrt{n}} \right|
$$

$$
\leq \frac{\|Q(\mathbf{Y} - f(\mathbf{X})) - (Q(f^0(\mathbf{X}) - f(\mathbf{X}) + \nu))\|_2}{\sqrt{n}}
$$

$$
= \frac{\|Q(f^0(\mathbf{X}) + \mathbf{H}\delta + \nu - f(\mathbf{X})) - (Q(f^0(\mathbf{X}) - f(\mathbf{X}) + \nu))\|_2}{\sqrt{n}}
$$

$$
= \frac{\|Q(f^0(\mathbf{X}) - f(\mathbf{X}) + \mathbf{X}b + (\mathbf{H}\delta - \mathbf{X}b) + \nu) - (Q(f^0(\mathbf{X}) - f(\mathbf{X}) + \nu))\|_2}{\sqrt{n}}
$$

$$
\leq \frac{\|Q\mathbf{X}b\|_2}{\sqrt{n}} + \frac{\|Q(\mathbf{H}\delta - \mathbf{X}b)\|_2}{\sqrt{n}}
$$

From Lemma 1 below, we have that $\|b\|_2 = \mathcal{O}(\|\delta\|_2/\sqrt{p})$ and hence using (7)

$$
\frac{\|Q\mathbf{X}b\|_2}{\sqrt{n}} \leq \frac{1}{\sqrt{n}}\lambda_{\max}(Q\mathbf{X})\|b\|_2 = \mathcal{O}\left(\|\delta\|_2\frac{\max(\sqrt{n}, \sqrt{p})}{\sqrt{np}}\right) = \mathcal{O}\left(\frac{\|\delta\|_2}{\min(\sqrt{n}, \sqrt{p})}\right).
$$

By Lemma 2 below, the second term behaves as

$$
\frac{1}{\sqrt{n}}\|Q(\mathbf{H}\delta - \mathbf{X}b)\|_2 = \mathcal{O}_{\mathbb{P}}\left(\frac{\|\delta\|_2}{\sqrt{p}}\right),
$$

which concludes the proof. $\qquad\square$

Lemma 1 (Parts of Lemma 6 in Ćevid et al., 2020). *Assume that the confounding model (1) satisfies the assumptions (4), (5) and (6). Then we have,*

$$
\|b\|_2^2 = \|\mathbb{E}[XX^T]^{-1}\mathbb{E}[XH^T]\delta\|_2^2 \leq \mathrm{cond}(\Sigma_E) \cdot \frac{\|\delta\|_2^2}{\lambda_{\min}(\Gamma)^2} = \mathcal{O}\left(\frac{\|\delta\|_2^2}{p}\right).
$$

Lemma 2. *Under the conditions of Theorem 1,*

$$
\frac{1}{n}\|Q(\mathbf{H}\delta - \mathbf{X}b)\|_2^2 = \mathcal{O}_{\mathbb{P}}\left(\frac{1}{p}\right)
$$

Proof. Observe that $\frac{1}{n}\|Q(\mathbf{H}\delta - \mathbf{X}b)\|_2^2 \leq \frac{1}{n}\|Q\|_{op}^2\|\mathbf{H}\delta - \mathbf{X}b\|_2^2$, so it suffices to show that $\frac{1}{n}\|\mathbf{H}\delta - \mathbf{X}b\|_2^2 = \mathcal{O}_{\mathbb{P}}\left(\frac{1}{p}\right)$. By Markov's inequality, it suffices to show

$$
\mathbb{E}\left[\frac{1}{n}\|\mathbf{H}\delta - \mathbf{X}b\|_2^2\right] = \mathcal{O}\left(\frac{1}{p}\right). \tag{14}
$$

For this, we follow the arguments of Guo et al. (2022). Our term $\mathbb{E}\left[\frac{1}{n}\|\mathbf{H}\delta - \mathbf{X}b\|_2^2\right]$ corresponds to Δ in (47) in A.4. there. We can follow the proof of (35) in Lemma 2 given in Section C.4 in Guo et al. (2022). For this, we write

$$
\frac{1}{n}\|\mathbf{H}\delta - \mathbf{X}b\|_2^2 = \frac{1}{n}\sum_{i=1}^{n}(\mathbf{H}_i^T\delta - \mathbf{X}_i^Tb)^2
$$

18

Hence,

$$
\begin{aligned}
\mathbb{E}\left[\frac{1}{n}\|\mathbf{H}\delta - \mathbf{X}b\|_2^2\right] &= \frac{1}{n}\sum_{i=1}^{n}\mathbb{E}[(\mathbf{H}_i^T\delta - \mathbf{X}_i^Tb)^2] \\
&= \mathbb{E}[(H^T\delta - X^Tb)^2] \\
&= \mathbb{E}[\delta^THH^T\delta - 2\delta^THX^Tb + b^TXX^Tb] \\
&= \delta^T\mathbb{E}[HH^T]\delta - 2\delta^T\mathbb{E}[HX^T]b + b^T\mathbb{E}[XX^T]b \\
&= \delta^T\mathbb{E}[HH^T]\delta - 2\delta^T\mathbb{E}[HX^T]\mathbb{E}[XX^T]^{-1}\mathbb{E}[XH^T]\delta + \delta^T\mathbb{E}[HX^T]\mathbb{E}[XX^T]^{-1}\mathbb{E}[XH^T]\delta \\
&= \delta^T\mathbb{E}[HH^T]\delta - \delta^T\mathbb{E}[HX^T]\mathbb{E}[XX^T]^{-1}\mathbb{E}[XH^T]\delta \\
&= \delta^T(I_q - \Gamma(\Gamma^T\Gamma + \Sigma_E)^{-1}\Gamma^T)\delta
\end{aligned}
$$

where we used the definition of b and (4). As in equation (134) in the supplementary materials in Guo et al. (2022), using Woodbury's identity, we have

$$
I_q - \Gamma(\Gamma^T\Gamma + \Sigma_E)^{-1}\Gamma^T = (I_q + \Gamma\Sigma_E^{-1}\Gamma^T)^{-1}.
$$

Let $C = \Sigma_E^{-1/2}\Gamma^T$ and $C = U_C D_C V_C^T$ be the singular values decomposition of C. Then, we have

$$
\begin{aligned}
\mathbb{E}\left[\frac{1}{n}\|\mathbf{H}\delta - \mathbf{X}b\|_2^2\right] &= \delta^T(I_q + \Gamma\Sigma_E^{-1}\Gamma^T)^{-1}\delta \\
&\leq \|\delta\|_2^2 \lambda_{\max}\left((I_q + \Gamma^T\Sigma_E^{-1}\Gamma)^{-1}\right) \\
&= \|\delta\|_2^2 \lambda_{\max}\left((I_q + C^TC)^{-1}\right) \\
&= \|\delta\|_2^2 \lambda_{\max}\left(V_C(I_q + D_C^TD_C)^{-1}V_C^T\right) \\
&= \|\delta\|_2^2(1 + \lambda_{\min}(D_C^TD_C))^{-1} \\
&= \|\delta\|_2^2(1 + \lambda_{\min}(C^TC))^{-1} \\
&\leq \|\delta\|_2^2\lambda_{\min}(C^TC)^{-1}
\end{aligned}
$$

Note that

$$
\begin{aligned}
\lambda_{\min}(C^TC) &= \min_{x\neq 0}\frac{x^TC^TCx}{x^Tx} \\
&= \min_{x\neq 0}\frac{x^T\Gamma\Sigma_E^{-1}\Gamma^Tx}{x^T\Gamma\Gamma^Tx}\frac{x^T\Gamma\Gamma^Tx}{x^Tx} \\
&\geq \lambda_{\min}(\Sigma_E^{-1})\lambda_{\min}(\Gamma\Gamma^T) \\
&= \lambda_{\max}(\Sigma_E)^{-1}\lambda_{\min}(\Gamma)^2
\end{aligned}
$$

Hence,

$$
\mathbb{E}\left[\frac{1}{n}\|\mathbf{H}\delta - \mathbf{X}b\|_2^2\right] \leq \|\delta\|_2^2\lambda_{\max}(\Sigma_E)\lambda_{\min}(\Gamma)^{-2} = \mathcal{O}\left(\frac{\|\delta\|_2^2}{p}\right)
$$

$\square$

Code: All the code used for this paper is available here: `https://github.com/markusul/SDForest-Paper`

R-package for *SDForests*: R-package SDModels provides software for non-linear spectrally deconfounded models: `https://github.com/markusul/SDModels`

References

Angrist, J. D., Imbens, G. W., & Rubin, D. B. (1996). Identification of Causal Effects Using Instrumental Variables. *Journal of the American Statistical Association*, *91*(434), 444–455.

Bai, J. (2003). Inferential Theory for Factor Models of Large Dimensions. *Econometrica*, *71*(1), 135–171.

Bowden, R. J., Bowden, R. J., & Turkington, D. A. (1990). *Instrumental variables* (No. 8). Cambridge university press.

Breiman, L. (1996). Bagging predictors. *Machine Learning*, *24*(2), 123–140.

Breiman, L. (2001). Random Forests. *Machine Learning*, *45*(1), 5–32.

Ćevid, D., Bühlmann, P., & Meinshausen, N. (2020). Spectral Deconfounding via Perturbed Sparse Linear Models. *J. Mach. Learn. Res.*, *21*(1).

Chevalley, M., Roohani, Y., Mehrjou, A., Leskovec, J., & Schwab, P. (2022). CausalBench: A Large-scale Benchmark for Network Inference from Single-cell Perturbation Data. *arXiv:2210.17283*.

Cinelli, C., & Hazlett, C. (2020). Making Sense of Sensitivity: Extending Omitted Variable Bias. *Journal of the Royal Statistical Society Series B: Statistical Methodology*, *82*(1), 39–67.

Fan, J., Lou, Z., & Yu, M. (2024). Are Latent Factor Regression and Sparse Regression Adequate? *Journal of the American Statistical Association*, *119*(546), 1076–1088.

Friedman, J. H. (2001). Greedy Function Approximation: A Gradient Boosting Machine. *The Annals of Statistics*, *29*(5), 1189–1232.

Gagnon-Bartsch, J. A., & Speed, T. P. (2012). Using control genes to correct for unwanted variation in microarray data. *Biostatistics*, *13*(3), 539–552.

Guo, Z., Ćevid, D., & Bühlmann, P. (2022). Doubly debiased lasso: High-dimensional inference under hidden confounding. *The Annals of Statistics*, *50*(3).

Hothorn, T. (2005). Survival ensembles. *Biostatistics*, *7*(3), 355–373.

Hothorn, T., & Zeileis, A. (2021). Predictive Distribution Modeling Using Transformation Forests. *Journal of Computational and Graphical Statistics*, *30*(4), 1181–1196.

Leek, J. T., & Storey, J. D. (2007). Capturing Heterogeneity in Gene Expression Studies by Surrogate Variable Analysis. *PLoS Genetics*, *3*(9), e161.

Li, B., Friedman, J., Olshen, R., & Stone, C. (1984). Classification and regression trees (CART). *Biometrics*, *40*(3), 358–361.

Meinshausen, N. (2006). Quantile Regression Forests. *Journal of Machine Learning Research*, *7*(35), 983–999.

Meinshausen, N., & Bühlmann, P. (2010). Stability Selection. *Journal of the Royal Statistical Society Series B: Statistical Methodology*, *72*(4), 417–473.

Pearl, J. (1980). *Causality: models, reasoning, and inference.* Cambridge University Press, New York, second edition, 2009a. Forthcoming.

Peters, J., Bühlmann, P., & Meinshausen, N. (2016). Causal inference by using invariant prediction: identification and confidence intervals. *Journal of the Royal Statistical Society. Series B (Statistical Methodology)*, *78*(5), 947–1012.

Replogle, J. M., Saunders, R. A., Pogson, A. N., Hussmann, J. A., Lenail, A., Guna, A., . . . Weissman, J. S. (2022). Mapping information-rich genotype-phenotype landscapes with genome-scale Perturb-seq. *Cell*, *185*(14), 2559–2575.

Scheidegger, C., Guo, Z., & Bühlmann, P. (2025). Spectral Deconfounding for High-Dimensional Sparse Additive Models. *To appear in ACM / IMS Journal of Data Science, early online access at https://dl.acm.org/doi/10.1145/3711116*.

Shen, X., Bühlmann, P., & Taeb, A. (2023). Causality-oriented robustness: exploiting general additive interventions. *arXiv:2307.10299*.

Stock, J. H., & Trebbi, F. (2003). Retrospectives: Who invented instrumental variable regression? *Journal of Economic Perspectives*, *17*(3), 177–194.

Taylor, J. M. (2011). Random Survival Forests. *Journal of Thoracic Oncology*, *6*(12), 1974–1975.

Ulmer, M., & Scheidegger, C. (2024). *SDModels: Spectrally Deconfounded Models.* R-package. Retrieved from `https://markusul.github.io/SDModels/`

Wilms, R., Mäthner, E., Winnen, L., & Lanwehr, R. (2021). Omitted variable bias: A threat to estimating causal relationships. *Methods in Psychology*, *5*, 100075.

Wright, M. N., & Ziegler, A. (2017). ranger: A Fast Implementation of Random Forests for High Dimensional Data in C++ and R. *Journal of Statistical Software*, *77*(1).